Large-eddy simulations of the Northeastern US coastal marine boundary layer

Lawrence C. Cheung[1], Colleen M. Kaul[2], Alan S. Hsieh[3], Myra L. Blaylock[1], Matthew J. Churchfield[4]

[1]Sandia National Laboratories, Livermore, CA 94550, USA
[2]Pacific Northwest National Laboratory, Richland WA 99354, USA
[3]Sandia National Laboratories, Albuquerque, NM 87185, USA
[4]National Renewable Energy Laboratory, Golden, CO 80401, USA

Author email: lcheung@sandia.gov

Abstract. In this study, large eddy simulations (LES) of offshore boundary layers near the Nantucket coast are performed using Nalu-Wind. The marine boundary layer conditions are chosen to match the predominantly unstable and neutral conditions measured by the Cape Wind platform. The appropriate domain, resolution, and boundary condition settings required for the LES are established through this work. Differences between stable and unstable cases are found in the wind speed profiles, averaged statistics, and wind spectra, and explained in terms of stratification effects.

1. Introduction

The recent development of offshore wind energy in the United States has driven a greater need to understand the wind resource and atmospheric characteristics of the US East Coast. Numerous previous studies of offshore wind measurements have examined sites in the North Sea [1, 2], but the characteristics of the Northeastern Atlantic coast can differ significantly. For instance, coastal low-level jets have been frequently observed at US locations [3] but are not as prevalent in other locations. Other weather phenomena, such as Nor'easters, are also specific to the region and need to be accounted for during the siting process.

Recent measurement campaigns of the Northeastern US coast have provided a series of wind data which can be used to understand the baseline atmospheric boundary layer and wind characteristics for potential offshore wind farms. Using a ship-borne Doppler lidar system, Pichugina *et al.* [4] were able to measure the wind profiles and vertical shear profiles in the Gulf of Maine. Archer *et al.* [5] used two measured data sets collected near Nantucket Sound to determine the expected atmospheric conditions in the marine boundary layer. They found that low-shear, unstable conditions were frequently observed, with strong seasonal variations and wind speed changes due to diurnal variation.

High fidelity CFD simulations can also be used to supplement measurements when studying the characteristics of the atmospheric boundary layer (ABL). Recent work by Kaul *et al.* [6] have shown that LES computations using Nalu-Wind can capture the neutrally and convectively unstable onshore ABL. In the current work, we demonstrate that the same approach can be used for offshore ABL simulations of the Northeastern Atlantic coast. The ABL simulations represent typical conditions as

Sandia National Laboratories is a multimission laboratory managed and operated by National Technology & Engineering Solutions of Sandia, LLC, a wholly owned subsidiary of Honeywell International Inc., for the U.S. Department of Energy's National Nuclear Security Administration under contract DE-NA0003525. SAND2020-5996C

measured by the Cape Wind meteorological tower [5], and illustrate the effects of varying degrees of thermal stratification.

1.1. Study objectives

The current work of simulating offshore marine boundary layers focuses on three major objectives. First, we will compute a series of neutral and unstable boundary layer simulations matching the shear, stability, and turbulence intensity (TI) characteristics of a measured offshore Northeastern US site. Secondly, computational domain, resolution, and boundary condition settings for these ABL simulations will be documented and discussed. Lastly, we will study the differences in ABL behavior due to stratification by comparing their wind profiles, averaged statistics, and spectra.

2. Methodology

In the following sections, we describe selected offshore conditions used in the offshore ABL simulations, as well as the computational approach used in each of the calculations.

2.1. Measured flow conditions

Measurements of the offshore coastal marine boundary layer, collected by the Cape Wind meteorological tower in Nantucket Sound, are used as the basis for this computational study. The Cape Wind platform collected wind measurements at 20m, 41m, and 60m above the mean water level, along with temperature and barometric measurements from the years 2003-2011. From the observations, Archer *et al.* [5] found that the marine boundary layer is predominantly unstable, with 61% of conditions classified as unstable, versus 21% neutral and 18% stable. The stratification of the marine boundary layer, as determined by the Obukhov length, also had a large impact on the wind speed profile, with flatter, non-logarithmic profiles seen during unstable conditions.

Table 1. Targeted ABL conditions.

Stability	Wind speed [m/s]	Wind dir [deg]	Turbulence Intensity
Neutral	5	225	0.055
Neutral	10	225	0.055
Neutral	15	225	0.065
Unstable	5	315	0.080
Unstable	10	315	0.075
Unstable	15	315	0.090

Using the measured distribution of stabilities, turbulent kinetic energy (TKE) and wind speeds from the Cape Wind platform reported in [5], six conditions were chosen as targets for the computational simulations in this study (see table 1). The neutral and unstable stratifications were chosen as the most representative of the measurement site, and three wind speeds from 5 m/s to 15 m/s were selected for each stability class. The TKE value for each condition was based on the median value of published data measured by the sonic anemometer at 20m elevation, and converted into a turbulence intensity (TI) value using the relation

$$TI = \sqrt{2/3 \times TKE}/\overline{U}_{horiz}(z)$$

where $\overline{U}_{horiz}$ is mean horizontal velocity. The wind direction for each condition was also chosen to be consistent with the Cape Wind observations, which show that neutral and stable conditions are associated strongly with south-southwesterly flow, while northwesterly flows are typically unstable flows during the colder seasons.

2.2. Nalu-Wind details

The current study of offshore ABL uses the unstructured, large eddy simulation (LES) code Nalu-Wind [7, 8], developed as a part of the US Department of Energy Exawind and Exascale computing

project. This code solves the incompressible Navier-Stokes equations with a low-Mach number approximation and a Boussinesq buoyancy model, along with the Coriolis forcing term. For the subgrid scale stresses, a one-equation, constant-coefficient turbulent kinetic energy model is used. An introduction to the Exawind program can be found in [7], and additional details on the numerical schemes and computational methodology in Nalu-Wind can be found in the online documentation [9].

2.3. Computational setup

In general, the computational methodology for the current study followed the best practices of previous ABL simulations using Nalu-Wind [6]. We assume that, with the appropriate boundary condition settings, the same general practices used for onshore ABL can be applied in an offshore setting as well. In particular, we choose to represent the air/ocean interface with a flat boundary with a small amount of surface roughness, which can be handled by the current wall model. A summary of the computational domain, mesh resolution, and applied boundary conditions is provided in table 2.

Two spatial domains, a large domain and a small domain, were used over the course of this study. The large spatial domain extended 6km in each horizontal direction and was used for full scale runs and capturing ABL statistics. This size was chosen in order to capture the large scale, coherent structures which may develop in boundary layer flows. The smaller spatial domain extended 1.5km in each horizontal direction and was used to determine the appropriate surface roughness and heat flux to match the target conditions. The vertical extent was 1km for the neutral conditions and 1.995km for the unstable conditions, and the latitude was set to 41.5 degrees for both domains.

The mesh resolution used in each simulation was chosen to balance the conflicting demands of capturing the unsteady flow features and the available computational resources. A uniform 10m resolution was used in the horizontal directions for all cases. In the vertical direction, the neutral simulations also used 10 m resolution, while for the unstable simulations, 7.5m resolution was used to capture the larger temperature and vertical velocity fluctuations due to heating. Supplementary studies using 6m vertical resolution showed negligible change in the boundary layer behavior, so the coarser vertical resolution was adopted for computational efficiency.

Table 2. Computational domain and boundary conditions. Domain sizes are given for the larger simulations.

Stability	Wind speed [m/s]	Domain size L×W×H [m]	Mesh resolution $\Delta x \times \Delta y \times \Delta z$ [m]	Surface roughness z_0 [m]	Surface heat flux [W/m^2]
Neutral	5	6000×6000×1000	10×10×10	0.0001	0
Neutral	10	6000×6000×1000	10×10×10	0.0001	0
Neutral	15	6000×6000×1000	10×10×10	0.0005	0
Unstable	5	6000×6000×1995	10×10×7.5	0.0005	15
Unstable	10	6000×6000×1995	10×10×7.5	0.0005	80
Unstable	15	6000×6000×1995	10×10×7.5	0.0050	120

2.3.1. Boundary and initial conditions. In both horizontal directions of the computational domain, periodic boundary conditions were applied. Monin-Obukhov similarity theory was used to determine the velocity and temperature profiles near the lower surface given a surface roughness height z_0 and the surface heat flux. Following previous practices, the initial temperature profile in all cases was a constant 300K until the specified inversion height of 650m in neutral cases and 1050m in unstable cases. The inversion layer thickness was 100m, and above this, the temperature linearly increased until it reached 308.75K at the upper boundary. At the upper surface of the domain, a potential flow based boundary condition is applied along with a normal temperature gradient of 0.003 K/m. The initial mean velocity profile was uniform throughout the domain with superimposed sinusoidal velocity perturbations of magnitude 1 m/s to promote the development of turbulence. For unstable cases, temperature perturbations of 0.8K magnitude were also applied below the inversion height.

Although the choice of the surface roughness z_0 and heat flux were chosen to match the measured conditions from Archer *et al.* [5], we can compare them to values found in the literature. Measurements of z_0 from the North Sea [10] also found typical surface roughness values of z_0 from 5×10^{-5} m to 5×10^{-3} m, which are consistent with values used in this study.

Similarly, the applied surface heat flux is consistent with values used in previous studies and experimental measurements. For instance, earlier LES studies [11] of ocean surface heating considered heat flux values up to 64 W/m^2 for moderately heated cases. Simulations of the Barents Sea [12], although at a higher latitude, suggest that the averaged ocean-atmosphere heat loss ranges from 37 W/m^2 to 130 W/m^2. These values are within the range applied to the current computations.

2.3.2. Simulation workflow. To find the appropriate conditions which match the targeted measure ABL characteristics in section 2.1, a series of initial LES computations were performed on the smaller 1.5 km ×1.5 km domain. Momentum source terms in Nalu-Wind were applied to ensure that the horizontally averaged velocity matched the desired geostrophic wind at the z=20 m height. These source terms are based on the difference between the desired wind velocity and the instantaneous horizontally averaged velocity and are only a function of time and height z. The surface roughness height and heat flux were adjusted until the averaged TI values matched the measured conditions. An additional goal for the unstable ABL cases was to minimize the shear exponent at the same height. Once acceptable conditions were found, the same BCs were applied on the large 6km×6km domain, where simulations were typically run for 15,000 seconds to remove initial transients, and then continued for another 3,000-5,000 seconds to collect averaged statistics and wind spectra.

3. Results

A large number of results from all six offshore ABL cases were collected, including averaged horizontal statistics, mean flow profiles, and wind spectra. Unsurprisingly, noticeable differences in the behavior between neutral and unstable cases were observed and are discussed below.

3.1. Horizontally averaged ABL statistics

A summary of all horizontally averaged ABL statistics is given in table 3. As expected, the averaged wind speed at z=20 m matches the desired geostrophic wind, although strong local variations are seen on an instantaneous basis (see section 3.2).

The comparison between the targeted and computed TI conditions is shown in figure 1(a). For the three neutral cases, the applied surface roughness values yield an ABL with TI levels very close to the desired values. For the unstable cases, the large domain simulations are able to match the target TI levels within 0.007.

Table 3. Simulated ABL results at z=20m height

Stability	Wind speed [m/s]	Turbulence Intensity	Shear exp. α	Friction vel. u_τ [m/s]	Obukhov length L [m]
Neutral	5.0	0.0550	0.0668	0.1503	5.655e+06
Neutral	10.0	0.0569	0.0638	0.3002	5.964e+05
Neutral	15.0	0.0645	0.0723	0.5055	2.007e+05
Unstable	5.0	0.0861	0.0222	0.1636	-2.911e+01
Unstable	10.0	0.0785	0.0229	0.3191	-4.116e+01
Unstable	15.0	0.0858	0.0632	0.6424	-2.608e+02

Comparisons for the wind shear of all six cases appear in figure 1(b). Here the shear exponent α is calculated assuming a power-law profile exists at the z_{FH}=20 m forcing height, such that $U(z) = U_{FH}(z/z_{FH})^{\alpha}$, where U_{FH} and z_{FH} are the values at the forcing height. For all three neutral cases, the shear exponent values were relatively similar, within the range $0.063 < \alpha < 0.073$. For the unstable boundary layers, the shear values for the 5 m/s and 10 m/s cases were noticeably lower, near α=0.022-

0.023. This corresponds to a much flatter velocity profile compared to the neutral cases. However, for the unstable 15 m/s case, the shear exponent α was much closer to neutral values, and consequently, its velocity profile at z=20 m bears a strong resemblance to the neutral case (see section 3.2). As discussed below, this similarity can be explained by examining the levels of stratification in the boundary layers.

In general, the stability of an atmospheric boundary layer can be quantified and classified using the Obukhov length L. This length depends on the friction velocity u_τ and is defined as

$$L = -\frac{u_\tau^3}{\frac{\kappa g}{T_0}\frac{H}{\rho C_p}} \approx -\frac{u_\tau^3}{\frac{\kappa g}{T_0}\overline{w'T'}} \quad (1)$$

where $\kappa = 0.41$ is the Kolmogorov constant, $g = 9.81$ m/s^2, $\rho = 1.164$ kg/m^3 is the density, H is the heat flux, and C_p is the specific heat capacity. The calculation of L is done using the average temperature flux $\overline{w'T'}$ at the ABL forcing height to match the previous experimental calculations. In this study, we also follow the conventions of [5] and categorize the boundary layers as neutral for $|L| > 500$, unstable for $-500 < L < -100$, and very unstable for $-100 < L < -5$.

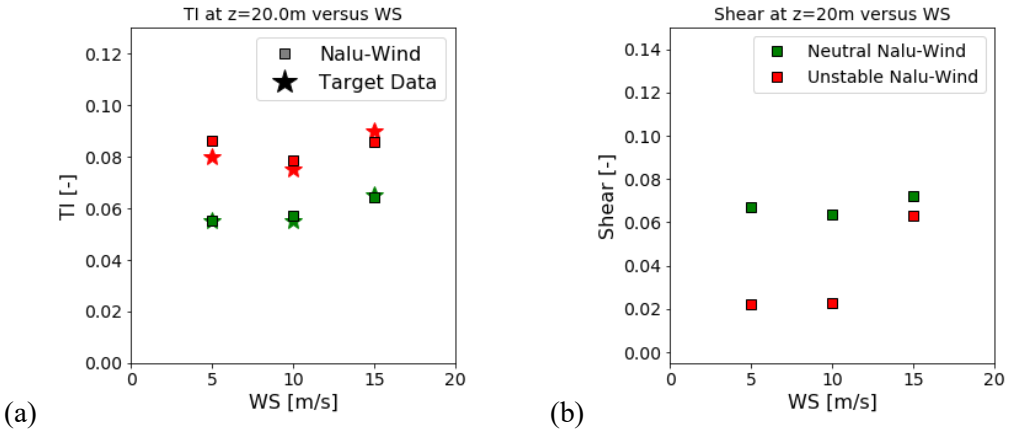

(a) (b)

Figure 1. (a) Comparison of the computed versus target TI conditions, and (b)sShear exponent versus wind speed (WS) for neutral and unstable conditions.

Figure 2 illustrates the relative atmospheric stability of each boundary layer based on the Obukhov length. While all cases with zero heat flux fall firmly in the neutral category, only the 5 m/s and 10 m/s unstable are classified as "very unstable". The remaining 15 m/s unstable case is classified only as "unstable" and borders the neutral regime.

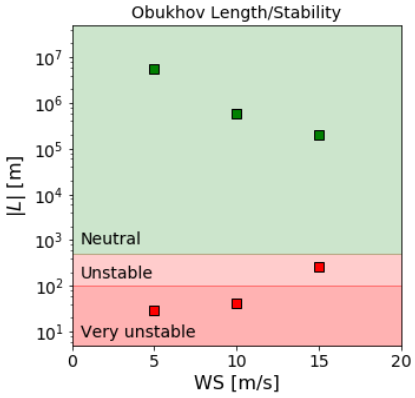

Figure 2. Classification of ABL stability based on Obukhov length L

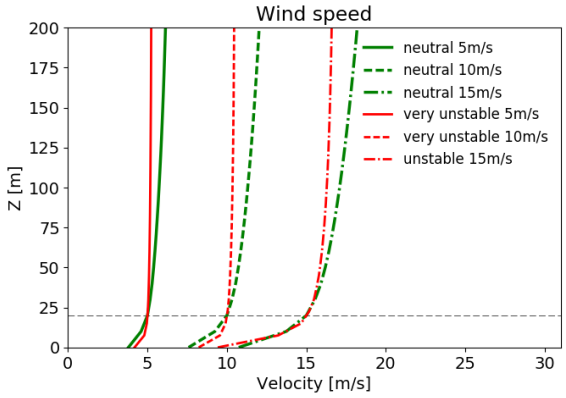

Figure 3. Averaged horizontal wind speed profile as a function of elevation

This difference between the unstable cases ultimately stems from the impact of heat flux and surface shear on the Obukhov length. As stated in equation (1), the Obukhov length is proportional to the cube of the friction velocity. However, the calculated friction velocity u_τ in all cases varied relatively linearly with wind speed. In order to achieve a similar "very unstable" stability state, the 15 m/s case would require a proportional increase in surface heat flux, on the order of 640-960 W/m^2. Applying such a large surface heat flux would require a larger domain and longer convergence times to accommodate the convective structures. Despite this difference in stability, the contrast in unstable behaviour is worth noting and examining further in the following sections.

3.2. Mean flow profiles

The variations of the wind and turbulence profiles are shown in figure 3 and figure 4, respectively. At the forcing height z=20 m, the horizontally averaged wind speeds are the same for the neutral and unstable cases. However, above that height the very unstable 5 m/s and 10 m/s profiles quickly flatten when compared to the neutral cases. More similarity is seen between the neutral and unstable 15 m/s profiles, especially for z<20 m, but some flattening of the unstable profiles is visible for higher heights. The decay of the turbulence profiles with elevation in figure 4 is again relatively similar for the neutral and unstable 15 m/s cases, while for the very unstable cases, the TI decrease is not as strong due to the higher relative surface heat flux and increased vertical transport of momentum.

Another noticeable difference between the unstable and neutral cases is illustrated by the wind veer comparison in figure 4. In all cases the same Coriolis force was applied for a latitude of 41.5° N, but the unstable boundary layers showed negligible wind direction change up to z=200 m. In contrast, the neutral boundary layer cases displayed relatively linear veer profiles, up to a 5° change for the first 200 m elevations in the neutral 5 m/s case.

The qualitative differences between the various stabilities and wind speeds can also be seen in the instantaneous velocity field images. In figure 5, the horizontal velocity magnitude is shown at the z=20 m plane for all six cases. The three neutral cases and unstable 15 m/s case in figure 5(a,c,e,f) all show patterns of narrow, high-speed and low-speed streaks through the boundary layer. However, the large-scale structures in the very unstable ABL cases of figure 5(b,d) display a different pattern. Cellular, rather than streaky patterns, are visible, with widths exceeding 1-2 km. The interior of these cellular patterns can be seen in the streamwise planes of vertical velocity shown in figure 6(b). These cellular patterns are associated with convective structures and updrafts due to surface heating. The strong vertical fluctuations are absent in the neutral cases (figure 6(a)).

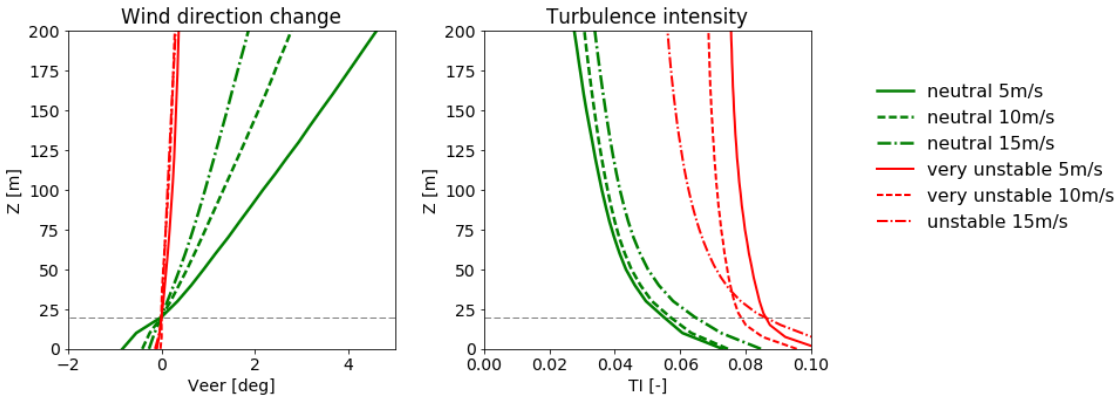

Figure 4. Left: comparison of the wind veer versus elevation, taken with respect to the wind direction at z=20m. Right: Comparison of the turbulence intensity change with height.

3.3. Wind spectra

In addition to the wind speed profiles and stability characteristics, data captured during the ABL simulations allows us to calculate the wind spectra $S_i(f)$ as a function of frequency f:

$$\int_0^\infty S_i(f)\ \mathrm{d}f = \sigma_i^2,$$

where σ_i^2 is the wind speed variance and the index $i = u, v, w$ denotes the longitudinal, lateral, or vertical velocity, respectively. The wind speed spectra provide some indication of the flow structures and unsteady characteristics in the boundary layer, and it is useful for determining the dynamic wind loads of turbines operating in the ABL.

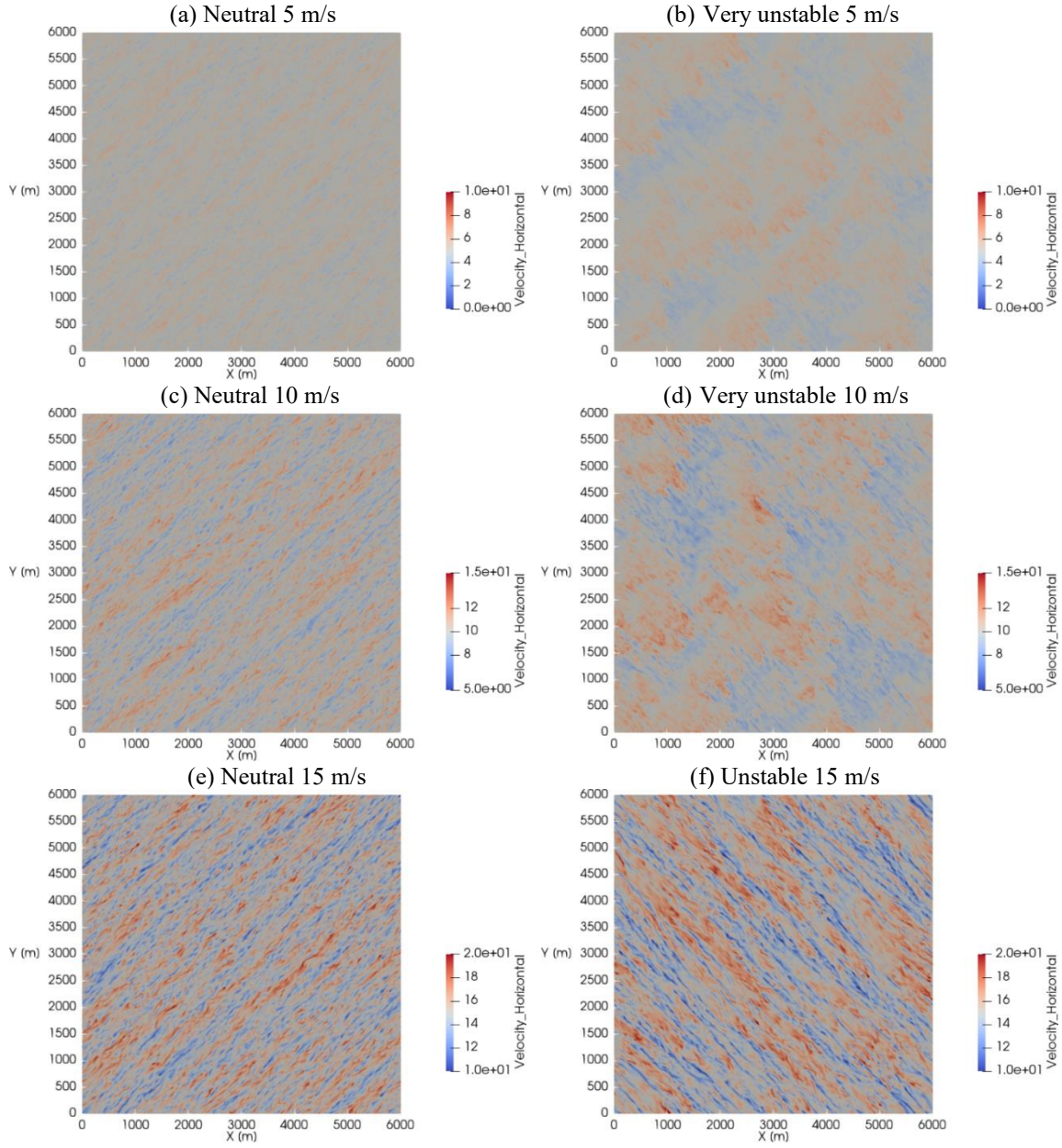

Figure 5. Instantaneous horizontal velocity at z=20 m plane. Note that the wind direction for the neutral cases in (a), (c) and (e) is from 225°, while for the unstable cases (b), (d), (f) it is from 315°.

To calculate the spectra, velocity data was gathered from the simulations at a frequency of Δt=0.5 seconds, divided into two bins of at least 4000 samples with 50% overlap, windowed and Fourier transformed. The spectra were further horizontally averaged using 144 equally spaced points on the z=20 m plane. The maximum resolvable frequency can also be estimated for each case. If we assume

that the smallest turbulent eddies in the flow convect with speed $0.6\overline{U}_{horiz}$, and require a minimum of N mesh elements to resolve, then the highest resolvable frequency f_{max} can be calculated as

$$f_{max} = \frac{0.6\ \overline{U}_{horiz}}{\mathrm{N}\Delta} \tag{2}$$

For the current cases, we use N=8 elements, and the mesh spacing $\Delta = 10\sqrt{2}$ m, in order to account for the flow orientation with the computational grid.

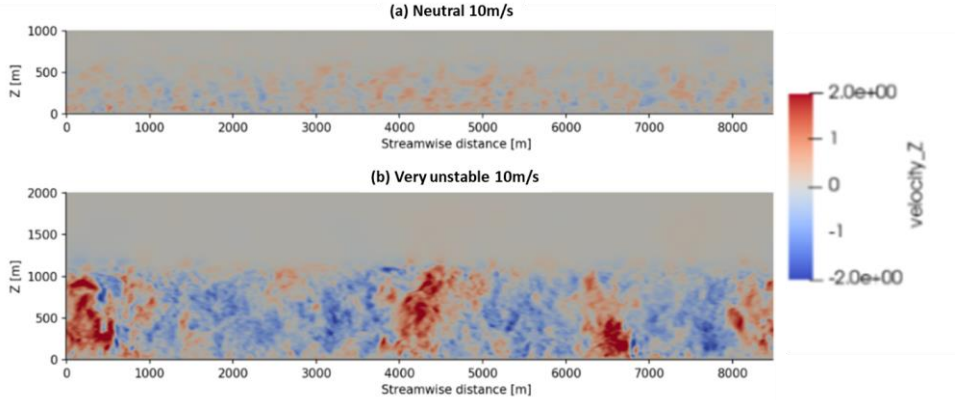

Figure 6. Instantaneous w velocity on the streamwise plane for the neutral and unstable 10 m/s case.

The wind spectra computed from the LES simulations can also be compared against previously developed analytical models. Although many such models currently exist, the Kaimal model [13] is a convenient choice which has been compared to numerous onshore and offshore measurements. The model for $S_i(f)$, when normalized against u_τ, can be expressed as

$$\frac{fS_i}{u_\tau^2} = \frac{a_i[fz/\overline{U}]}{(1 + b_i[fz/\overline{U}]^{\alpha_i})^{\beta_i}} \tag{3}$$

where the parameters a_i, b_i, α_i, β_i are given in table 4 below.

Table 4. Parameters for the Kaimal model spectra given in equation (3)

Velocity	a_i	b_i	α_i	β_i
$\boldsymbol{u}$	105.0	33.0	1	5/3
$\boldsymbol{v}$	17.0	9.5	1	5/3
$\boldsymbol{w}$	2.1	5.3	5/3	1

The comparison of the Kaimal model with the simulated spectra at the z=20 m plane are shown in figure 7. For the neutral cases, the velocity spectra from the computations follow the Kaimal model up to the spectral peak. The LES spectra captures the energy containing range and the location and magnitude of the S_u spectral peak. However, beyond the highest resolvable frequency f_{max}, the spectra are under-resolved and fail to capture the inertial range.

For the very unstable ABL cases, strong differences can be seen between the simulated spectra and the Kaimal model. In these two cases, the peak amplitude shifts to a much lower frequency than predicted by the Kaimal model, and the maxima of the S_u and the S_v spectra are approximately the same order. The shift to lower frequency in the energy containing ranges may be associated with the large-scale convective structures which arise due to the surface heating. In addition, the higher energy content of the S_w spectra may be due to increased vertical transport. However, because the Kaimal model (3) was calibrated for near-neutral flows, close agreement is not expected in these cases.

Lastly, for the wind spectra of the unstable case at 15 m/s run on the small domain, the spectral peak also exists at a lower frequency than the Kaimal predicted maximum, but the S_u and the S_v low frequency increases are not as prominent as in the 5 m/s and 10m/s cases. A small increase in the S_w spectra is also seen, similar to the other unstable cases.

4. Conclusions

In this study, we have simulated a series of neutral and unstable offshore marine boundary layers matching the typical characteristics as measured by the Cape Wind platform in Nantucket Sound. We documented the computational process used in the LES calculations, and the appropriate computational domain, resolution, and boundary condition settings that were applied.

Noticeable differences were observed between the neutral and very unstable ABL cases in this study. The very unstable boundary layers developed large convective structures due to the applied surface heating and flatter velocity profiles. While the neutral ABL wind spectra matches the Kaimal model closely, the very unstable cases show increased energy at lower frequencies. The unstable 15 m/s case was also found to be similar to the neutral ABL cases due to its less convective nature.

Acknowledgments

This research was supported by the Wind Energy Technologies Office of the US Department of Energy Office of Energy Efficiency and Renewable Energy. Sandia National Laboratories is a multimission laboratory managed and operated by National Technology & Engineering Solutions of Sandia, LLC, a wholly owned subsidiary of Honeywell International Inc., for the U.S. Department of Energy's National Nuclear Security Administration under contract DE-NA0003525. The views expressed in the article do not necessarily represent the views of the U.S. Department of Energy or the United States Government. SAND2020-5996C

References

[1] M. Türk, K. Grigutsch and S. Emeis, "The Wind Profile Above the Sea—Investigations Basing on Four Years of FINO 1 Data," *DEWI Mag,* vol. 33, pp. 12-16, 2008.

[2] A. Sathe, S. Gryning and A. Peña, "Comparison of the atmospheric stability and wind profiles at two wind farm sites over a long marine fetch in the North Sea," *Wind Energy,* vol. 14, no. 6, pp. 767-780, 2011.

[3] C. G. Nunalee and S. Basu, "Mesoscale modeling of coastal low-level jets: implications for offshore wind resource estimation," *Wind Energy,* vol. 17, no. 8, pp. 1199-1216, 2014.

[4] Y. Pichugina, W. Brewer, R. Banta, A. Choukulkar, C. Clack, M. Marquis, B. McCarty, A. Weickmann, S. Sandberg, R. Marchbanks and R. Hardesty, "Properties of the offshore low level jet and rotor layer wind shear as measured by scanning Doppler Lidar," *Wind Energy,* vol. 20, no. 6, pp. 987-1002, 2017.

[5] C. Archer, B. Colle, D. Veron, F. Veron and M. J. and Sienhiewicz, "On the predominance of unstable atmospheric conditions in the marine boundary layer offshore of the US northeastern coast," *Journal of Geophysical Research: Atmospheres,* vol. 121, no. 15, pp. 8869-8885, 2016.

[6] C. Kaul, S. Ananthan, M. Churchfield, J. Mirocha, L. Berg and R. Rai, "Large eddy simulations of idealized atmospheric boundary layers using Nalu-Wind," in *NAWEA WindTech Conference Proceedings, Oct. 13-16, 2019*, Amherst, MA, 2019.

[7] M. A. Sprague, S. Ananthan, G. Vijayakumar and M. Robinson, "ExaWind: A multi-fidelity modeling and simulation environment for wind energy," in *NAWEA WindTech Conference Proceedings, Oct. 13-16, 2019*, Amherst, MA, 2019.

[8] S. P. Domino, "Sierra Low Mach Module: Nalu Theory Manual 1.0," Sandia National Laboratories SAND2015-3107W, 2015.

[9] "Nalu-Wind Documentation," [Online]. Available: https://nalu-wind.readthedocs.io/en/latest/index.html.

[10] P. K. Taylor and M. Y. Yelland, "The dependence of sea surface roughness on the height and steepness of the waves," *Journal of physical oceanography,* vol. 31, no. 2, pp. 572-590, 2001.

[11] B. C. Pearson, A. L. Grant, J. A. Polton and S. E. Belcher, " Langmuir turbulence and surface heating in the ocean surface boundary layer," *Journal of Physical Oceanography,* vol. 45, no. 12, pp. 2897-2911, 2015.

[12] M. Årthun and C. Schrum, "Ocean surface heat flux variability in the Barents Sea.," *Journal of Marine Systems,* vol. 83, no. 1-2, pp. 88-98., 2010.

[13] J. C. J. Kaimal, "Turbulence spectra, length scales and structure parameters in the stable surface layer," *Boundary-Layer Meteorology,* vol. 4, no. 1-4, pp. 289-309, 1973.

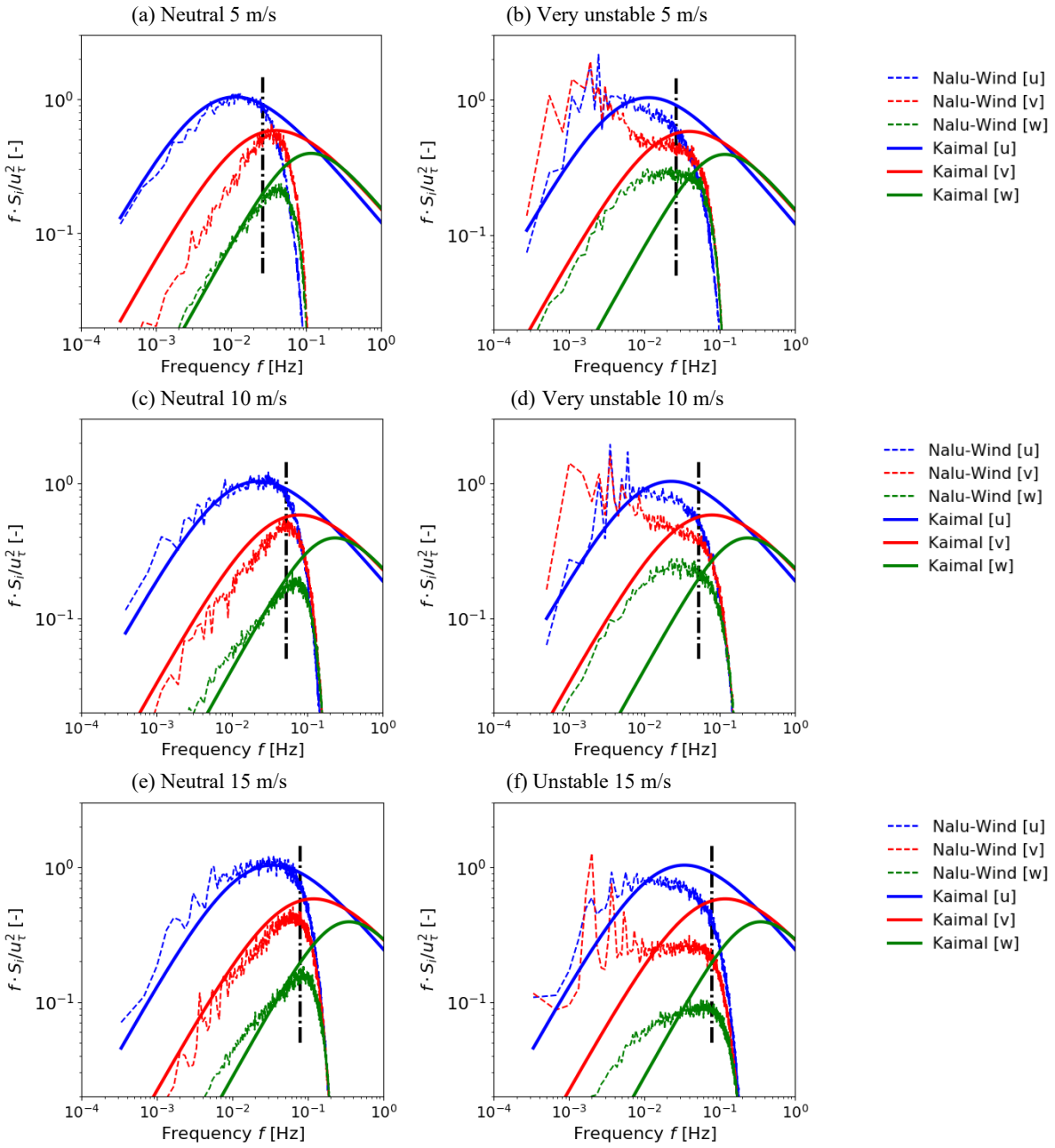

Figure 7. Normalized wind spectra for Nalu-Wind and the Kaimal model given in equation (3). The vertical dashed black line corresponds to maximum resolved frequency f_{max} given in equation (2).